JOURNAL OF ENVIRONMENTAL SCIENCES 97 (2020) 75–84

Available online at www.sciencedirect.com

ScienceDirect

www.elsevier.com/locate/jes

JES JOURNAL OF ENVIRONMENTAL SCIENCES

www.jesc.ac.cn

Catalytic ozonation treatment of papermaking wastewater by Ag-doped $NiFe_2O_4$: Performance and mechanism

Junyu Zhao[1,2], *Jiashun Cao*[1,2], *Yujie Zhao*[3], *Teng Zhang*[1,2], *Di Zheng*[1,2], *Chao Li*[1,2,*]

[1] *Key Laboratory of Integrated Regulation and Resource Development on Shallow Lakes, Ministry of Education, Hohai University, Nanjing 210098, China*

[2] *College of Environment, Hohai University, Nanjing 210098, China*

[3] *China United Engineering Corporation Limited, Zhejiang 310000, China*

ARTICLE INFO

Article history:
Received 1 November 2019
Revised 3 April 2020
Accepted 8 April 2020
Available online 7 June 2020

Keywords:
Papermaking wastewater
Secondary effluent
Nickel ferrite
Ag-doping
Catalytic ozonation

ABSTRACT

The catalytic ozonation treatment of secondary biochemical effluent for papermaking wastewater by Ag-doped nickel ferrite was investigated. Ag-doped catalysts prepared by sol-gel method were characterized, illustrating that Ag entirely entered the crystalline of $NiFe_2O_4$ and changed the surface properties. The addition of catalyst enhanced the removal efficiency of chemical oxygen demand and total organic carbon. The results of gas chromatography-mass spectrometer, ultraviolet light absorbance at 254 nm and three-dimensional fluorescence excitation-emission matrix suggested that aromatic compounds were efficiently degraded and toxic substances, such as dibutyl phthalate. In addition, the radical scavenging experiments confirmed the hydroxyl radicals acted as the main reactive oxygen species and the surface properties of catalysts played an important role in the reaction. Overall, this work validated potential applications of Ag-doped $NiFe_2O_4$ catalyzed ozonation process of biologically recalcitrant wastewater.

Introduction

The papermaking industry is the third largest water consumption industry after the metal and chemical industry over the world. The paper mills had emitted abundant wastewater which contained suspended particles, strong color, chlorine-containing compounds and recalcitrant organics (Ginni et al., 2014; Pokhrel and Viraraghavan, 2004). The complex compounds cannot be treated efficiently by the conventional biochemical processes, which may cause serious environmental pollution. Additionally, hazardous raw materials were employed in the production process. For example, di-*n*-butyl phthalate (DBP), as one of the phthalate esters (PAEs) was widely used in the papermaking industry due to its good stability, cohesiveness and waterproofing. However, DBP was poisonous and hardly degraded by microorganism, so it can be detected in the secondary effluents (Sun et al., 2008; Zhang et al., 2010). Thus, it is imperative to carry out the advanced treatment of biochemical effluents.

Ozonation oxidation process, with little hazardous by-products generation, is considered as a promising advanced oxidation process (AOPs) for DBP or other recalcitrant organics treatment. In order to enhance oxidation and treatment ability of intermediates, heterogeneous catalytic ozonation were employed to accelerate the decomposition of ozone to generate the hydroxyl radicals which has stronger oxidation ability. However, there are also some problems that need to be solved for the widespread application of the catalytic ozonation pro-

* Corresponding author at:
E-mail: lichao0609@163.com (C. Li).

https://doi.org/10.1016/j.jes.2020.04.014
1001-0742/

cess. For example, the degradation efficiency and intermediates of the actual wastewater needed to be investigated. On the other hand, the reusability and stability of the catalysts should be paid more attention for lower cost.

As one of the composite metal oxides, spinel oxides have excellent physical and chemical properties and excellent catalytic performance (Jaafarzadeh et al., 2017; Sundararajan et al., 2017). Spinel oxides can be divided into iron spinel, aluminum spinel, chrome spinel, cobalt spinel, etc. according to the composition of metal elements. Iron spinel, as a magnetic nanoparticle, due to its special superparamagnetic property and the large specific surface area has attracted many attentions (Ren et al., 2012). Some investigation reported that iron spinel, as a heterogeneous catalyst, can promote the ozone decomposition and have good catalytic performance for aromatic compounds degradation (Zhang et al., 2015; Zhao et al., 2013). And iron spinel can be easily separated by utilizing external magnetic field and exhibited satisfactory stability (Zhang et al., 2017). To further promote the value of spinel ferrite in water treatment, metal ions modification was employed to improve the catalytic property (Lv et al., 2010). The metal doped catalysts have more Lewis acid sites on the surface, which owned more hydroxyl groups on the surface and improves the activity of the catalyst (Ren et al., 2016).

Silver, compared with other metals, has higher stability, splendid electrical and thermal conductivity which may make it a promising dopant to improve the properties of $NiFe_2O_4$, as an ozonation catalyst for actual wastewater treatment (Krejčíková et al., 2012; Wang et al., 2018). On the other hand, Ag acts as decomposition center for ozone to effectively promote ozone decomposition to generate reactive oxygen species (ROS) (Lin et al., 2000) and accelerates the electron transfer between catalyst and ozone (Ling et al., 2016). However, the efficiency of Ag-doped $NiFe_2O_4$ for catalytic ozonation of secondary effluents of papermaking wastewater remains unclear and needs to be explored.

The main objectives of the present study were to (1) synthesize and characterize Ag-doped $NiFe_2O_4$ as a heterogeneous ozonation catalyst, (2) investigate the chemical oxygen demand (CODcr) degradation of papermaking wastewater and evaluate the kinetics of catalytic ozonation with different Ag-doped catalysts, (3) analyze the main kinds of pollutants in the papermaking wastewater and their degradation by gas chromatography-mass spectrometry (GC–MS) and ultraviolet light absorbance at 254 nm (UV_{254}), (4) study the possible degradation pathway of containments.

1. Materials and methods

1.1. Materials and chemicals

$Ni(NO_3)_3{\cdot}6H_2O$, $Fe(NO_3)_3{\cdot}9H_2O$, $AgNO_3$, sodium sulfite, hydrochloric acid (HCl), *tert*-butyl alcohol ($C_4H_{10}O$, TBA), sodium phosphate (Na_3PO_4), and sodium hydroxide (NaOH) were all analytical grade. The papermaking wastewater to be treated was obtained from a biochemical effluent of a current running treatment system in Jiangsu province, China and the water quality was CODcr 100–150 mg/L, total nitrogen 4–11 mg/L, total phosphorus 0.1–0.5 mg/L, ammonia nitrogen 2–8 mg/L, and suspended solids 4–10 mg/L. Deionized (DI) water was used for all experiments.

1.2. Catalyst synthesis

The sol-gel method was employed to synthesize the pristine and Ag-doped $NiFe_2O_4$ catalysts. In a typical run, a 40 mL aqueous solution containing 6.66 mmol $Fe(NO_3)_3{\cdot}9H_2O$, as well as aliquots of $Ni(NO_3)_3{\cdot}6H_2O$ and $AgNO_3$ (molar ratio Ag : Ni : Fe = 2x : 1-x : 2) was slowly added into 50 mL egg white with vigorous stirring for 30 min, then the mixture was evaporated in the water bath at 80°C. The amount of $AgNO_3$ was controlled at an initial molar loading of 1%, 2%, and 5% relative to Ni (the prepared catalysts was marked as $Ag_{0.02}Ni_{0.99}Fe_2O_4$, $Ag_{0.04}Ni_{0.98}Fe_2O_4$, $Ag_{0.06}Ni_{0.97}Fe_2O_4$ and $Ag_{0.1}Ni_{0.95}Fe_2O_4$, respectively). The mixture was further calcined at 550°C for 5 hr, and quenched in a mixture of ice and water. The final product was washed with DI water and dried, resulting in magnetic powders as the catalyst materials.

1.3. Ozonation processes

The applied ozone was produced from oxygen by an ozone generator (WH-H-Y10, Woke, China) and controlled at 5 mg/L. In a typical experiment, 1.0 L of papermaking wastewater and 0.1 g of catalyst were added into a 1.5 L glass reactor at room temperature (25 ± 2°C) and mixed well by a magnetic stirrer, the mixing gas was fed into the reactor at the flow rate of 0.6 L/min and the off-gas was adsorbed by 20 vol.% KI solution. The initial pH was adjusted by 0.1 mol/L NaOH or HCI solution. Samples were collected and spiking with Na_2SO_3 solution to quench the residual at given time intervals. Finally, the samples were filtered with syringe filters (cellulose acetate, 0.45 μm) for analysis.

1.4. Analytical methods

The surface micrograph was characterized by a scanning electron microscopy (SEM, FEI quanta 250, USA). X-ray diffraction (XRD) patterns of catalysts were characterized by X'Pert PRO MPO MPD (Panalytical, Holland). Fourier-transform infrared spectroscopy (FTIR) was conducted with Nicolet Nexus 470 (Thermo, USA) to determine FTIR spectra in medium infrared (400–4000 cm^{-1}). The specific surface area of catalysts was characterized and analyzed by ASAP 2020 plus HD 88 (Micromeritics, USA). The magnetic strength of catalysts was measured and analyzed by MPMS XL-7 (Quantum Design, USA). X-ray photoelectron spectroscopy (XPS, ESCALAB 250Xi, ThermoFisher, USA) was used for qualitative valence analysis of surface elements of the catalysts. Gas chromatography-mass spectrometry (GC–MS, GC(7820)-MS(5975), Agilent, USA) was used to detect the organic compounds before and after the treatment. Three-dimensional excitation and emission matrix (3D-EEM) spectrofluorometer (F-7000, Hitachi, Japan) was employed to determine the fluorescent dissolved organic matter.

2. Results and discussion

2.1. Catalyst characterization

Scanning electron microscopy images of catalysts are shown in Fig. 1. Due to the oxidation and gasification of organic matters during the calcination process, the magnetic porous catalysts had similar morphology, smooth surface covered with coarser particles. The similar morphology between raw $NiFe_2O_4$ and Ag-doped $NiFe_2O_4$ suggested that Ag doping had negligible effects on the surface properties of catalysts. Meanwhile, more loose states were observed on the surface of catalysts with the increase of Ag dosage, possibly due to the doping Ag hindered the enrichment ability of egg white with metal ions.

The Brunauer-Emmett-Teller (BET) analysis of $NiFe_2O_4$ and Ag-doped $NiFe_2O_4$ were shown in Table 1. The total pore volumes of all catalysts were around 0.165 cm^3/g. The specific surface area of $Ag_{2x}Ni_{1-x}Fe_2O_4$ (x = 0, 1, 2, 3 and 5 mol.%) were 45.03, 58.53, 57.97, 57.65 and 58.89 m^2/g, respectively, suggesting that Ag doping can enhance the specific surface area

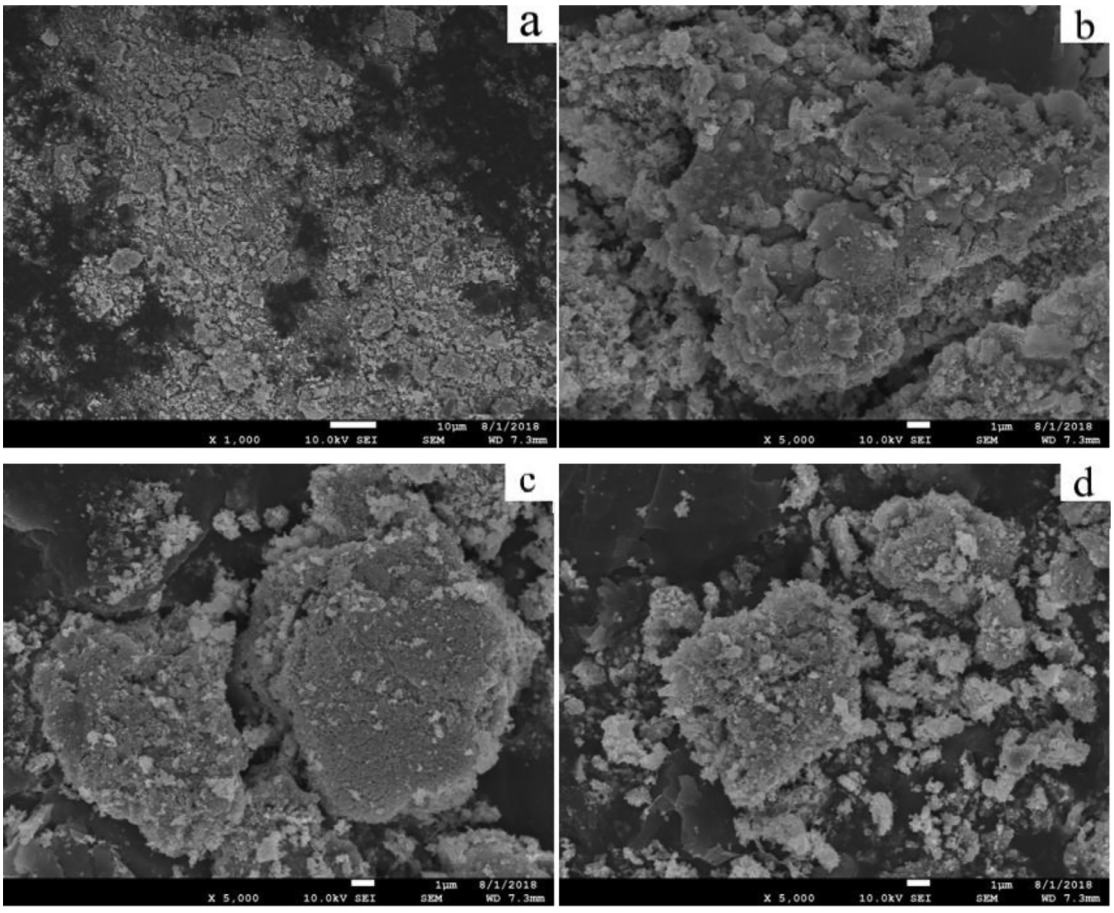

Fig. 1 – Scanning electron micrograph of (a) $NiFe_2O_4$, (b) $Ag_{0.02}Ni_{0.99}Fe_2O_4$, (c) $Ag_{0.06}Ni_{0.97}Fe_2O_4$ and (d) $Ag_{0.1}Ni_{0.95}Fe_2O_4$.

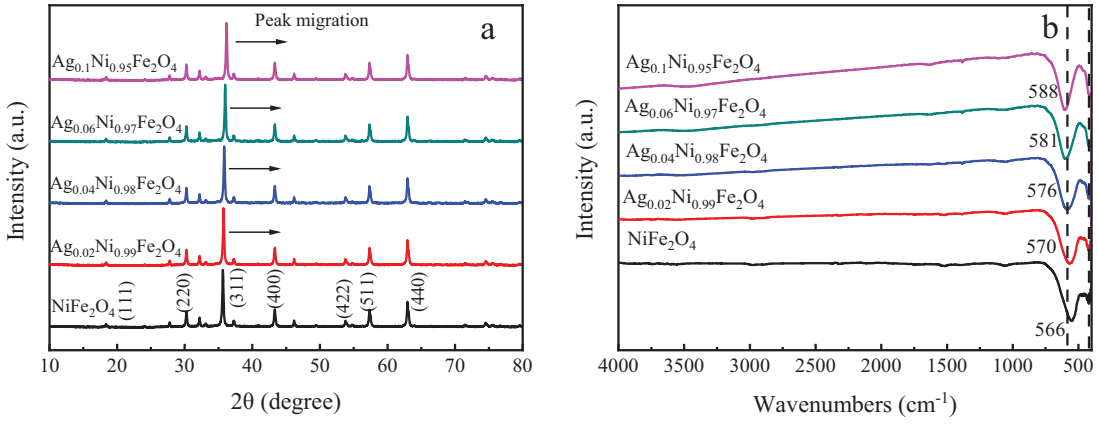

Fig. 2 – (a) X-ray diffraction and (b) Fourier-transform infrared spectra of different catalysts.

Table 1 – Brunauer-Emmett-Teller (BET) surface area, total pore volume and pore radius of catalysts.

Catalyst	BET (m^2/g)	Total pore volume (cm^3/g)	Pore radius (nm)
$NiFe_2O_4$	45.025	0.1740	9.03
$Ag_{0.02}Ni_{0.99}Fe_2O_4$	58.536	0.1658	10.99
$Ag_{0.04}Ni_{0.98}Fe_2O_4$	57.968	0.1625	8.98
$Ag_{0.06}Ni_{0.97}Fe_2O_4$	57.652	0.1559	9.68
$Ag_{0.1}Ni_{0.95}Fe_2O_4$	58.885	0.1605	9.99

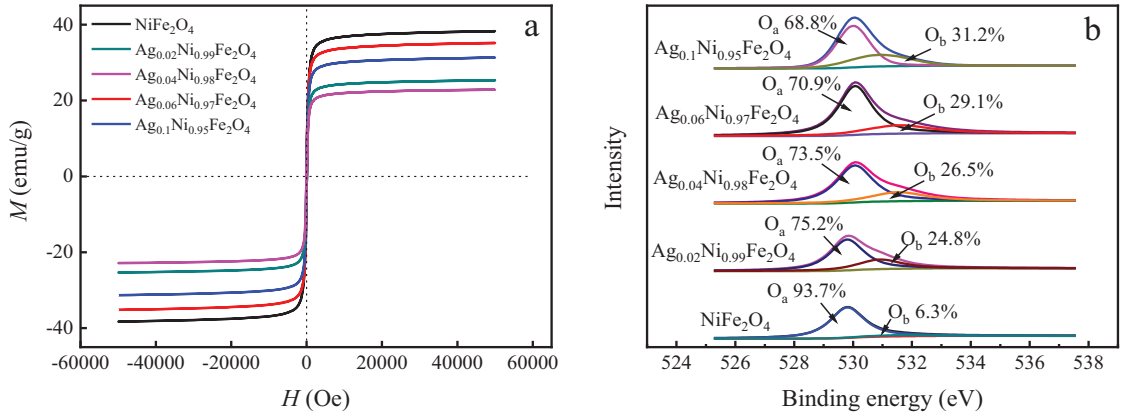

Fig. 3 – (a) Vibrating sample magnetometer and (b) X-ray photoelectron spectroscopy (XPS) O1s of different catalysts. *M*: magnetization; *H*: magnetic field strength; O_a: lattice oxygen of metal oxides; O_b: adsorbed oxygen or the surface hydroxyl species.

and $Ag_{0.1}Ni_{0.95}Fe_2O_4$ had the largest surface area which was beneficial to increase the contact area of catalysts and ozone molecules during the reaction.

XRD analysis were applied to examine the crystalline phases and properties of the catalysts. Compared with the raw $NiFe_2O_4$, no extra peak for the Ag-doped $NiFe_2O_4$ was observed (Fig. 2a), indicating that the crystalline phase of the pristine spinel structural did not change and no impurity was produced with the Ag doping up to 5 mol.%. However, comparing to $NiFe_2O_4$, the diffraction peaks of Ag-doped $NiFe_2O_4$ shifting to slightly higher 2θ values with increasing degree of Ag-doping indicated that Ag completely entered the crystal lattice of $NiFe_2O_4$. It is reported that the tetrahedral sites were more possible to be occupied by the low-valence ions and the extent of the shift mainly caused by the loading of Ag^+ ions, the radii of Ag^+ and Ni^{2+} ions, and the different bonding energy of Ni-O-Fe and Ag-O-Fe (Ren et al., 2016; Verwey and Heilmann, 1947).

FTIR spectra in the range 450–4000 cm^{-1} was employed to investigate the surface properties of as-prepared catalysts (Fig. 2b). With the increase of Ag dosage, the adsorption peaks of $Ag_{2x}Ni_{1-x}Fe_2O_4$ (x = 0, 1, 2, 3 and 5 mol.%) was observed at 566, 570, 574, 581 and 588 cm^{-1}, respectively. These typical adsorption bands can be attributed to the intrinsic vibration mode of Fe^{3+}-O^{2-} in tetrahedral sites for all the spinel ferrites (Allafchian et al., 2015; Waldron, 1955). The doping of Ag may took place the sites of Ni in the crystal structure, resulting in the formation of Ag-O-Fe oxo-bridged bimetallic linkage and possibly destroyed the original balance of chemical bonds of Ni-O-Fe (Mohammed et al., 2012).

As the Fig. 3a shown, the values of saturation magnetization for $Ag_{2x}Ni_{1-x}Fe_2O_4$ (x = 0, 1, 2, 3 and 5 mol.%) were 38.28, 25.34, 22.88, 35.20 and 31.33 emu/g, respectively, suggesting that with slight drop of saturation magnetization, the catalyst still exhibited a satisfactory magnetism to be separated from solution easily.

To obtain information concerning the interaction between Ag and $NiFe_2O_4$, detail scans of O 1 s core level had been recorded in Fig. 3b. Two distinct oxygen species at binding energies of 530.3 and 531.5 eV have been identified in the O 1 s spectra, representing the lattice oxygen of metal oxides (O^{2-}, denoted as O_a) and adsorbed oxygen or the surface hydroxyl species (denoted as O_b) of the catalysts, respectively (Kruse and Chenakin, 2011; Marikutsa et al., 2010). It is reported that surface hydroxyl groups and lattice oxygen were both the reactive oxygen species and Ag doping might provide more active sites in the oxidation reaction (Saaedi et al., 2016). With the increase of Ag dosage, it can be found that the binding energies of lattice oxygen became lower. Lower binding energies were associated with reduction to a lower oxidation state or an increased electron density (Suresh et al., 2014). Due to the oxygen has a constant value, the lower binding energies represented higher electron density, which favored initiation of the activation of ozone due to the electrophilic property of ozone molecules (Wei et al., 2017).

2.2. *Catalytic oxidation of papermaking wastewater*

The CODcr and total organic carbon (TOC) degradation of papermaking wastewater by O_3 alone, $NiFe_2O_4/O_3$ and Ag-doped $NiFe_2O_4/O_3$ systems are illustrated in Fig. 4a-b. Ozone-free control experiments were conducted to detect the effect of adsorption of catalyst surfaces and the removal efficiency by $NiFe_2O_4$, $Ag_{0.02}Ni_{0.99}Fe_2O_4$, $Ag_{0.04}Ni_{0.98}Fe_2O_4$, $Ag_{0.06}Ni_{0.97}Fe_2O_4$ and $Ag_{0.1}Ni_{0.95}Fe_2O_4$ in 60 min were all less than 5%, indicating that containments were essentially degraded during the ozonation experiments, not by the adsorption.

The O_3 alone system presented an inefficient CODcr degradation of papermaking wastewater performance, only 22% removal in the initial 40 min and 23% removal in 60 min, indicating that the pollutants in papermaking wastewater were hardly removed by O_3 alone system. Contrastively, the CODcr degradation of papermaking wastewater by $NiFe_2O_4$, $Ag_{0.02}Ni_{0.99}Fe_2O_4$, $Ag_{0.04}Ni_{0.98}Fe_2O_4$, $Ag_{0.06}Ni_{0.97}Fe_2O_4$ and $Ag_{0.1}Ni_{0.95}Fe_2O_4$ were 53%, 58%, 62%, 65% and 70% in 60 min, respectively. The TOC degradation efficiency showed the same trend as CODcr removal, and the 5 mol.% Ag-doped $NiFe_2O_4$ showed the highest mineralization efficiency, increased by 50% compared with ozone alone process, better than copper-cerium oxide supported alumina whose TOC degradation efficiency was increased by 35.5% in 60 min, indicating that containments was degraded into reductive product after the oxidation process and have a promising application for wastewater treatment.

Clearly, as the Ag loading increased, the removal of CODcr was enhanced and $Ag_{0.1}Ni_{0.95}Fe_2O_4$ showed the best catalytic ability, which was about twice higher than the ozone alone. The results showed that CODcr removal efficiency was enhanced significantly by the catalysts, and the performance was further boosted by the addition of Ag. These results suggested that the dosage of catalyst may increase the amounts of active sites of surface ·OH and Ag doping might provide more active sites for more surface hydroxyl groups, which enhanced the decomposition of ozone molecules.

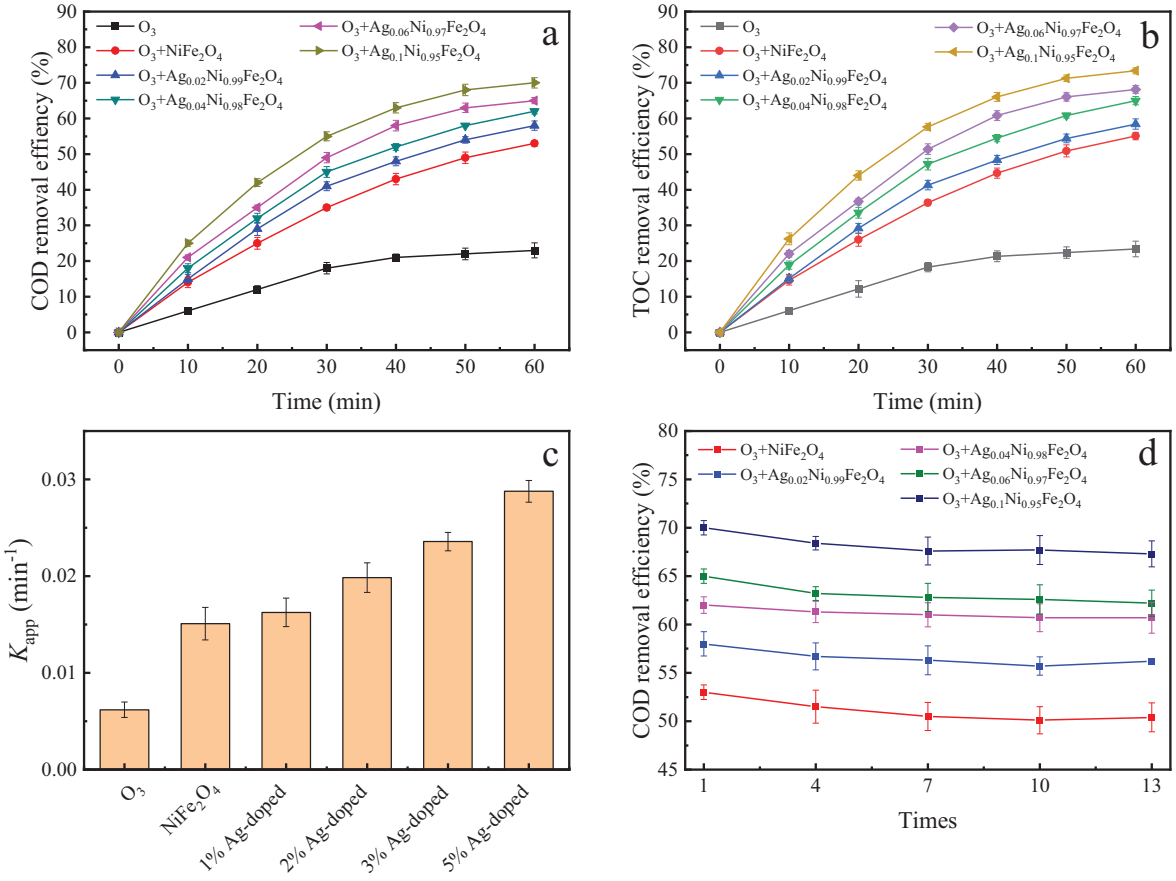

Fig. 4 – (a) Chemical oxygen demand (CODcr) degradation efficiency, (b) total organic carbon (TOC) removal efficiency, (c) the calculated pseudo-first-order rate constant (K_{app}), and (d) CODcr degradation efficiency after 60 min of reaction for thirteen successive cycles of different catalysts.

The degradation kinetic of CODcr can be described by pseudo-first-order rate law and the calculated rate constants were determined by fitting the Eq. (1).

$$\ln \frac{C_0}{C} = K_{app} \times t \quad (1)$$

where the K_{app} (min^{-1}) is the pseudo-first-order rate constant, C_0 (mg/L) and C (mg/L) are the CODcr concentrations initially and at the reaction time t (min), respectively. The rate constants of different ozonation system are presented in Fig. 4c. The initial rate constants of CODcr degradation were 0.0619, 0.0151, 0.0163, 0.0198, 0.0236 and 0.0288 min^{-1} in the O_3 alone, $NiFe_2O_4/O_3$ and $Ag_{2x}Ni_{1-x}Fe_2O_4/O_3$ systems, respectively. Among these, $Ag_{0.1}Ni_{0.95}Fe_2O_4$ has the highest rate constant of CODcr degradation, which were 4 and 2 times of the ozone alone and $NiFe_2O_4/O_3$ system, respectively. The initial kinetics of CODcr degradation were greatly affected by the amounts of Ag-doping and highest Ag-doping concentration achieved the largest reaction rate constant in ozonation system by enhancing the ozone decomposition to produce more hydroxyl radicals.

In addition, the catalytic ozonation performance for CODcr degradation in the presence of dissolved Ag, Ni and Fe leaching out from the $Ag_{0.1}Ni_{0.95}Fe_2O_4$ was also investigated, essentially the same as in the ozone alone system, suggesting that the homogeneous catalytic ozonation of released ions is not predominant. The stability tests of catalysts were conducted as shown in Fig. 4d. The degradation efficiencies of CODcr by $Ag_{0.02}Ni_{0.99}Fe_2O_4$, $Ag_{0.04}Ni_{0.98}Fe_2O_4$, $Ag_{0.06}Ni_{0.97}Fe_2O_4$ and $Ag_{0.1}Ni_{0.95}Fe_2O_4$ were reduced by 5.1%, 7.4%, 3.6%, 7.0% and 6.4%, respectively, after thirteen successive cycles of wastewater degradation experiments, indicating that Ag-doped catalysts with low ion leaching showed superb stability during the catalytic ozonation system.

The catalytic activity of the raw and Ag-doped $NiFe_2O_4$ was further determined in a series of catalyst concentrations (0–200 mg/L) to identify the optimum catalyst dosage and presented in Fig. 5a. The CODcr degradation efficiency was enhanced with the increase dosage from 0 to 100 mg/L. However, further increase of dosage showed an unfavorable effect on the degradation. The phenomenon was caused by the decrease of active sites due to the aggregation of catalysts and the leached-out Fe ions may act as a scavenger of hydroxyl radicals from the high dosage of catalysts (Ding et al., 2017; Yang et al., 2019). Among these catalysts, the $Ag_{0.1}Ni_{0.95}Fe_2O_4$ with the dosage of 100 mg/L illustrated the highest removal efficiency (~70% in 60 min) and the maximum rate constant (~0.0288 min^{-1}).

As a critical environmental parameter, the pH value is important in ozone alone and catalytic ozonation system, it not only affects the ozone mass transfer and decomposition, but also have effects on catalyst surface properties and the pK_a of organic compounds (Li et al., 2010; Ma et al., 2005). Seen from Fig. 5b, the CODcr degradation was enhanced with the increase of the initial pH in the ozone alone system, mainly

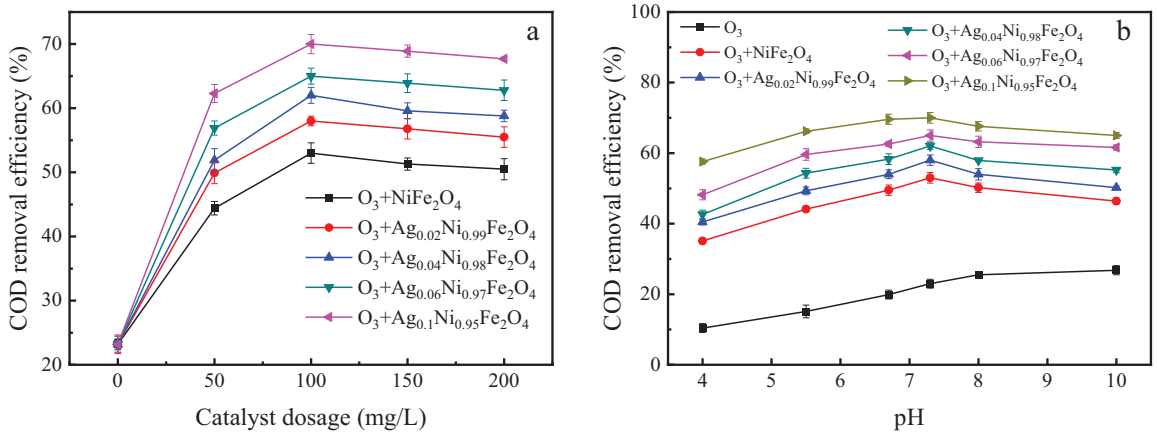

Fig. 5 – (a) Catalyst dosages and (b) pH condition effects of oxidation process with different catalysts.

due to that aqueous hydroxide in alkaline condition can enhance the decomposition of ozone and promote the generation of hydroxyl radicals (Zhao et al., 2009). However, different from the ozone alone system, the highest removal efficiency was achieved around the pH of the point of zero charge (pH_{pzc}) of catalyst, which played an important role in promoting O_3 decomposition and ·OH production (Yuan et al., 2013). When the pH condition was lower or higher than the pH_{pzc} of catalyst, the catalyst surface presents protonated or deprotonated state just as (Eqs. (2)-(3). The results were consistent with pervious investigation showing that uncharged surface hydroxyl groups promote ·OH generation from aqueous ozone (Qi et al., 2009).

$$Me - OH + H^+ \rightarrow MeOH_2^+ \ (pH < pH_{pzc}) \quad (2)$$

$$Me - OH + OH^- \rightarrow MeO^- + H_2O \ (pH > pH_{pzc}) \quad (3)$$

2.3. *Degradation of organic containments during the catalytic ozonation process*

The changes of several pollutants in papermaking wastewater before and after catalytic ozonation process were measured and calculated from GC–MS, and the result was shown in Table 2.

A total of 19 organic compounds were detected in the biochemical effluent of papermaking wastewater. The aromatics and the short-chain esters (i.e., 38.98% and 14.96%) were the main organic compounds before the degradation, respectively. Notably, the content of DBP, as one of priority pollutants on the national blacklist, was 9.93% and the content of DEBP was 9.11%. After the catalytic oxidation reaction, macromolecular organics were degraded into small molecular organics. The content of aromatic compounds decreased to 10.43%, the content of hydrocarbons increased to 71.56% and DBP or DBEP were not detected, indicating that catalytic ozonation can effectively degrade aromatic compounds in wastewater. Meanwhile, nitrogen-containing organic matter was not detected in the effluent, which may be due to the breakage of the C-N bond in the organic matter (Chen et al., 2008).

The UV_{254} revealed the aromaticity and unsaturation of the organic containments in the wastewater (Zhou et al., 2011; Wei et al., 2019). The papermaking wastewater samples for UV_{254} were collected at 0, 5, 10, 20, 30 and 60 min were 3.372, 1.138, 0.482, 0.374, 0.193 and 0.029 cm^{-1}, respectively. The high UV_{254} removal, up to 99.1% in 60 min, indicated that the pollutants with the C=O bond and C=C bond can be degraded effectively under the catalytic ozonation condition, which was consistent with the GC–MS.

Three-dimensional excitation-emission matrix spectroscopy and fluorescence regional integration (FRI) were employed to verify the different types of dissolved organic matter (DOM) and characterize them quantitatively, and the results were shown in Fig. 6. Three fluorescence peaks can be identified from the 3D-EEM spectra. Peak A was located at the excitation/emission (Ex/Em) wavelength of 280 nm/310 nm and was attributed to tyrosine and proteins. The peak at Ex/Em of 280 nm/350 nm (Peak B) was described as tryptophan and proteins. Peak C at Ex/Em of 235 nm/310 nm was described as the tyrosine. Peak identification of 3D-EEM spectra showed that the main fluorescent component of dissolved organic nitrogen (DON) was tyrosine-like protein, while the humic acids was the main fluorescent component of dissolved organic carbon (DOC).

According to previous study, the 3D-EEM peaks can be divided into five regions, I, II, III, IV and V. Regions I and II are related to aromatic protein-like fluorophores. Regions III and V are associated with fulvic acid-like and humic acid-like organic matter. In additional, Region IV is related to soluble microbial products (SMPs) (Li et al., 2019; Zhang et al., 2020).

The normalized integration volumes (NIV) of each region for influent and effluent of oxidation process are presented in Fig. 7. Before the oxidation process, the NIV of five regions were 0.51, 0.57, 0.43, 2.29 and 1.44 AU·nm^2·L/mg, respectively. After ozone catalytic oxidation, the NIV intensity decreased significantly. SMPs in Region IV are mainly composed of tryptophan and protein (Chen et al., 2003), therefore, the compounds in Regions I, II and IV belonged to fluorescent DON. The NIV of Region I decreased from 0.51 AU·nm^2·L/mg in the influent to 0.12 AU·nm^2·L/mg in the effluent and 77.09% aromatic protein was removed. The NIV of Region II and IV were decreased by 76.84% and 82.08%, respectively, and 80.43% of the fluorescent DON was removed in total. Fulvic acids in Region III and humic acids in Region V are typical fluorescent DOC. The removal efficiency of fulvic acids and humic acid were 57.69% and 85.45% and that of fluorescent DOC was 79.06%. Among the compounds in DOC, humic acids were effectively removed through the catalytic ozonation process, leading to significant DOM removal efficiency.

After the oxidation treatment, decreases were observed in the percentage of SMPs and humic acids, from 43.56% to 38.91%, and from 27.49% to 19.94%, respectively. The proportion of tyrosine increased from 9.86% to 11.26%, and that of fulvic acids increased from 8.21% to 17.33%. The percentage

Table 2 – Gas chromatography-mass spectrometry of biochemical effluent from papermaking wastewater before and after the reaction.

Number	Organic compounds	Relative molecular mass	Pre-reaction content (%)	Post-reaction content (%)
1	Ethyl acetate	88	/	5.78
2	Cyclohexanone	98	/	3.07
3	(+/-)-3-Hydroxy-gamma-butyrolactone	102	3.26	/
4	Trifluoro-*p*-tolunitrile	102	1.16	/
5	Ethylbenzene	106	/	6.51
6	Para-xylene	106	/	3.92
7	(S)-5-Hydroxymethyldihydrofuran-2-one	116	7.31	/
8	Ethyl butyrate	116	/	7.08
9	Trimethylheptane	142	/	8.61
10	2,4-Di-*tert*-butylphenol	155	7.05	/
11	Isobutyl valerate	158	/	2.08
12	γ-Decalactone	170	4.39	/
13	4,5-Dimethyloctane	173	/	19.02
14	*n*-Heptadecane	180	1.38	14.44
15	1,5,5-Trimethyl-6-acetylmethylcyclohexene	206	3.96	/
16	2,6,10,14-Tetramethylpentadecane	240	2.17	/
17	Phytane	254	2.40	/
18	Palmitic acid	256	6.87	/
19	Octadecane	268	1.52	29.50
20	7,9-Di-*tert*-butyl-1-oxaspiro[4.5]deca-6,9-diene-2,8-dione	276	4.54	/
21	Diisobutyl phthalate	278	9.11	/
22	Oleamide	281	7.51	/
23	Dibutyl phthalate	278	9.93	
24	Stearic acid	284	7.22	/
25	3,5-Dicyclohexyl-4-hydroxybenzoic acid methyl ester	316	4.76	/
26	Diisooctyl phthalate	390	6.97	/
27	Octacosanol	410	8.48	/

The symbol / means that the organic compounds were not detected and the symbol (+/-) means racemate.

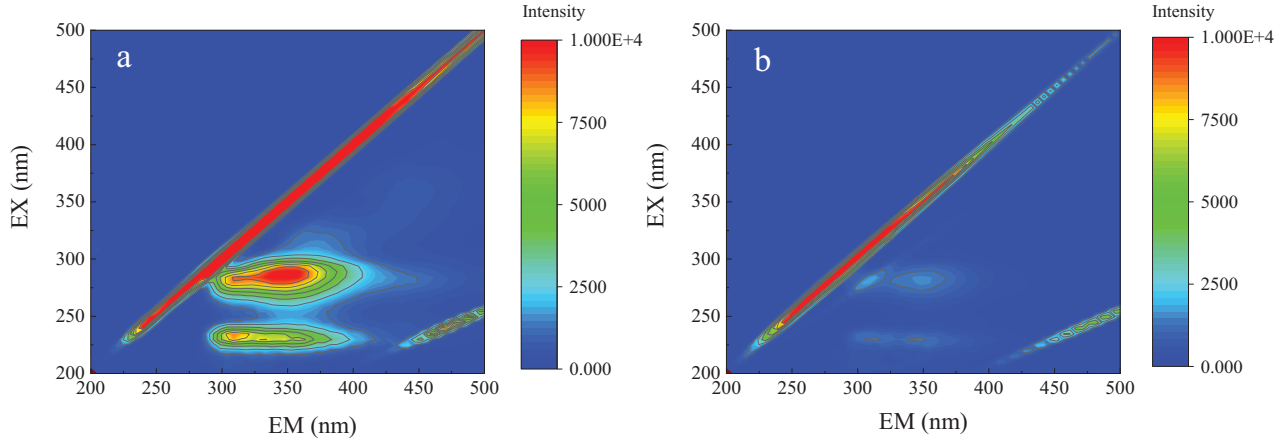

Fig. 6 – Three-dimensional excitation and emission matrix spectra of water samples of (a) secondary effluent and (b) effluent after catalytic ozonation process. EX: excitation wavelength; EM: emission wavelength.

of each region in the effluent was in the order of: Region IV > Region V > Region III > Region II > Region I.

2.4. *Surface redox properties of Ag-doped $NiFe_2O_4$ during catalytic ozonation process*

A series of approaches were performed to investigate the surface and redox properties of the catalyst. Compared with the un-doped $NiFe_2O_4$, the Ag doping significantly enhanced the density of surface hydroxyl groups of catalysts. The 5 mol.% Ag doping $NiFe_2O_4$ had the maximum surface hydroxyl density, which was consistent with the best CODcr degradation performance. To confirm whether the degradation of CODcr follow the hydroxyl radical theory, TBA as a ·OH scavenger was used to prevent the generation of hydroxyl radicals (Sui et al., 2011). As the Fig. 8 shown, the inhibitory effects of TBA in both uncatalyzed homogeneous and catalytic ozonation confirmed that the catalytic ozonation of CODcr degradation occurred

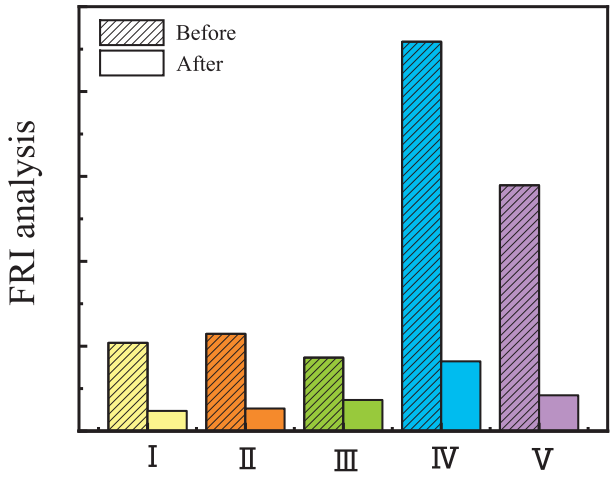

Fig. 7 – Fluorescence regional integration (FRI) analysis of the water samples before and after the catalytic ozonation treatment. I and II are related to aromatic protein-like fluorophores. III and V are associated with fulvic acid-like and humic acid-like organic matter. IV is related to soluble microbial products.

through reaction with ·OH and the degradation efficiency of CODcr declined progressively with the incremental addition of phosphate which prevented the surface hydroxyl groups producing radicals, indicating that surface hydroxyl groups are essential for the catalytic ozonation to promote CODcr degradation (Sui et al., 2010). Therefore, it is reasonable to propose that the surface hydroxyl groups of catalyst played the critical role during the catalytic ozonation process through producing hydroxyl radicals.

The catalytic activity of solid catalysts was reported related to the multiple components and multivalence of the metal, which were beneficial for the catalyst to undergo the redox reaction, promoting generation of the hydroxyl radicals (Nawrocki and Kasprzyk-Hordern, 2010). To study the electron transfer processes of the Ag-doped catalyst, XPS was used to detect the changes of the Ag, Fe and Ni elements before and after the catalytic ozonation reaction, and the results are shown in Fig. 9.

The XPS signals of 367.3 and 368.2 eV of the Ag 3d spectra were assigned to Ag^+ and Ag^0, respectively (Liu et al., 2017). Ag was exclusively present in the +1-oxidation state before the ozonation experiment. After reaction, a significant fraction of zero valent Ag species (i.e., 21.9%) was observed as indicated by the shift of the XPS spectra, suggesting that Ag underwent a reduction to generate reactive oxygen species. The characteristic peak of Ni 2p3/2 could be deconvoluted to Ni^{2+} (856.9 eV) and Ni^{3+} (863.7 eV). The relative quantity of Ni^{2+} decreased from 88.7% to 71.5%, while that of Ni^{3+} increased from 11.3% to 29.5% after the degradation experiments, suggesting that electrons were transferred from Ni^{2+} to ozone molecules, resulting in the generation of Ni^{3+} and O_3^-, which were the intermediates of the reaction. The peaks of Fe2p level at 711.07 and 724.37 eV were corresponding to Fe 2p3/2 and Fe 2p1/2 before and after the ozonation process, respectively. The analysis of Fe 2p3/2 photoelectron peak for the different oxidation states of Fe is difficult because of the huge background, but it is reasonable to judge the chemical state by the binding energies between the principal peak and satellite peak (Mittal et al., 2006). The characteristic satellite at around 8.4 eV above the main peak confirmed the existence of Fe^{3+} state and ruled out the any Fe^{2+} state in the structure (Nawale et al., 2011).

Thus, the results indicated that the Ag and Ni both participated in the catalytic ozonation process as primary redox active sites, and the reactions increased by the coexistence of their multiple oxidation states in the decomposition of ozone, involving the redox process of Ag^+-Ag^0-Ag^+ and Ni^{2+}-Ni^{3+}-Ni^{2+} (Balasamy et al., 2011).

XPS analysis of the O 1 s spectra observed that Ag doping changes the surface oxygen coordination of the catalysts. A sharp decrease of relative intensity of O_a was observed for $Ag_{0.1}Ni_{0.95}Fe_2O_4$ after degradation (i.e., from 68.8% to 55.9%), which the relative contents of O_b increased from 31.2% to 44.1%, implying that adsorbed and lattice oxygen both participated in the redox reaction during the oxidation process. The decrease of the surface lattice oxygen may be due to the adsorption of ozone on the catalyst surface, the formation of surface hydroxyl groups and the reaction that consumed the lattice oxygen (Legube and Leitner, 1999).

2.5. *Proposed reaction mechanism*

The heterogeneous catalytic ozonation process is being used as a novel type of advanced oxidation technology for the degradation of industrial wastewater. This process uses a catalyst to promote ozone decomposition to generate reactive oxygen species for better treatment. This work has illustrated

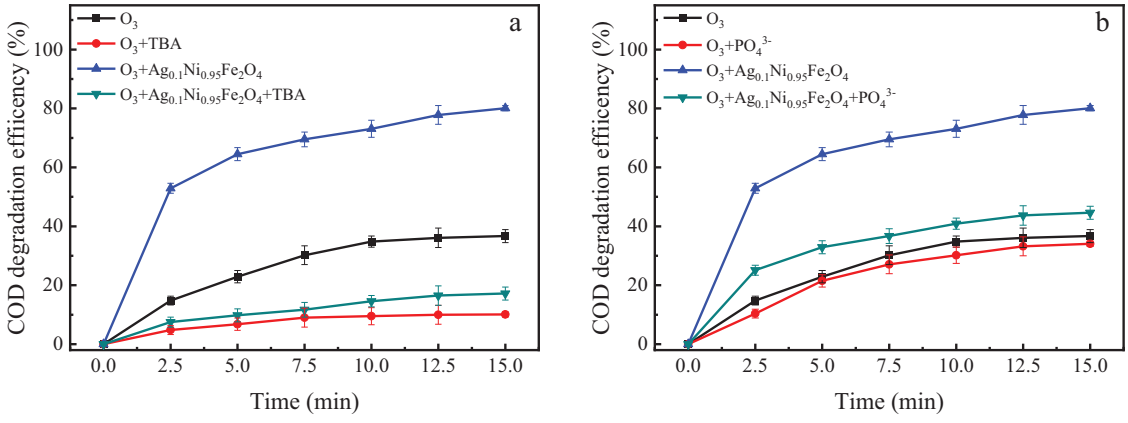

Fig. 8 – Effects of (a) *tert*-butyl alcohol (TBA, 100 mg/L) and (b) phosphate (100 mg/L) concentration on CODcr degradation with 0.5%Ag-$NiFe_2O_4$.

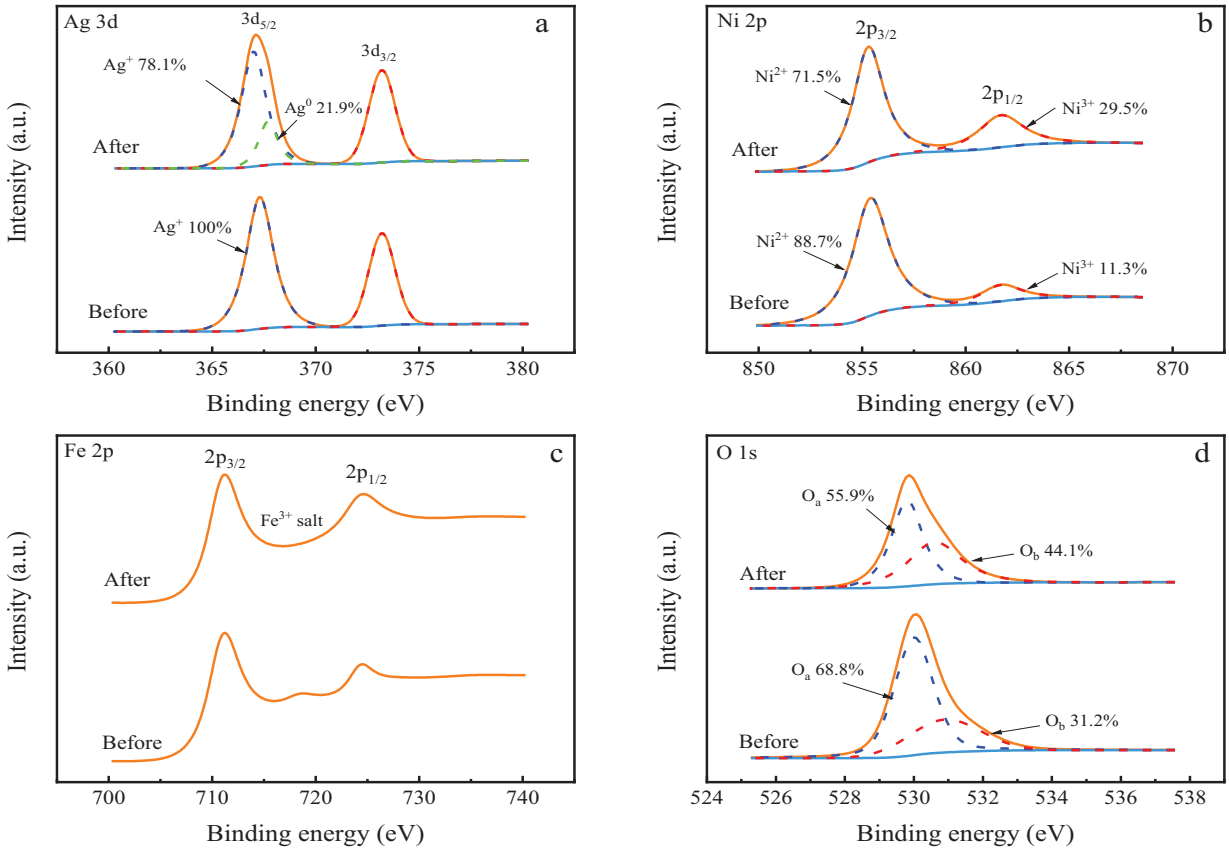

Fig. 9 – XPS of (a) Ag 3d, (b) Ni 2p, (c) Fe 2p and (d) O 1 s for 5%Ag-$NiFe_2O_4$ before and after catalytic ozonation process.

the importance of the surface hydroxyl groups on $NiFe_2O_4$ to enhance the ozone adsorption and the decomposition to generate hydroxyl radicals. The $NiFe_2O_4$ catalytic ozonation process can be described in a few general steps. At the first step, ozone was adsorbed by the hydroxyl groups on the surface, then Ni served as the active sites to transfer electron to the caught ozone for decomposing to the target $HO_2^{\cdot-}$ and $O_2^{\cdot-}$. In the next step, A chain reaction happened to $HO_2^{\cdot-}$ to produce the hydroxyl radicals, meanwhile the Ni^{3+} turned to Ni^{2+} by the lattice oxygen to maintain the electrostatic balance. Finally, O_2 replenished the lattice oxygen defects on catalyst surface and made sure the sustained supply of oxygen and activity.

On the other hand, Ag doping affected the surface and redox properties of the catalysts, and significantly accelerated the catalytic ozonation process. According to XPS results, Ag was doped into the $NiFe_2O_4$ in the formation of Ag^+ while both Ag^0 and Ag^+ were observed after the ozonation experiments, indicating the redox active role of Ag sites. Due to its superior electron transport properties, Ag can boost electron transfer with rapid turnover cycling of Ag^+-Ag^0-Ag^+. Based on previous investigation and experimental observation, we proposed that during the ozonation process, Ag(I) may act as an electron shuttle by mediating the electron transfer between Ni(II) and O_3 (Eqs. (4)–(11)).

$$Ni(II)Fe_2O_4 - OH^- + O_3 \rightarrow Ni(II)Fe_2O_4 - OH^- - O_3 \quad (4)$$

$$Ni(II)Fe_2O_4 - OH^- - O_3 \rightarrow Ni(III)Fe_2O_4 + HO_2^- + O_2^- \quad (5)$$

$$HO_2^- + O_3 \rightarrow O_2^- + O_2 + OH \quad (6)$$

$$4Ni(III)Fe_2O_4 + 2O^{2-} \rightarrow 4Ni(II)Fe_2O_4 + 2O_2 \quad (7)$$

$$O_2 + 4e^- \rightarrow 2O^{2-} \quad (8)$$

$$Ag(I)Ni(II)Fe_2O_4 - OH^- + O_3 \rightarrow Ag(I)Ni(II)Fe_2O_4 - OH^- - O_3 \quad (9)$$

$$Ag(I)Ni(II)Fe_2O_4 - OH^- - O_3 \rightarrow Ag(0)Ni(III)Fe_2O_4 - OH^- - O_3 \quad (10)$$

$$Ag(0)Ni(III)Fe_2O_4 - OH^- - O_3 \rightarrow Ag(I)Ni(III)Fe_2O_4 + HO_2^- + O_2^- \quad (11)$$

3. Conclusions

In this study, $Ag_{2x}Ni_{1-x}Fe_2O_4$ (x = 0, 1, 2, 3 and 5 mol.%) were prepared by sol-gel method and characterized by several methods and the addition of catalyst can significantly improve the removal efficiency. Dosage of catalyst and the pH condition were also important factors affecting the degradation performance, and the optimal operating conditions were determined as 100 mg/L at pH 7.3. To probe the changes of organic pollutants before and after the treatment, GC–MS and UV_{254} were employed and the results suggested that compounds with unsaturated bond or benzene rings were highly removed with the Ag-doped $NiFe_2O_4/O_3$ system, which provided a new reference for the catalytic treatment of biochemical effluent for papermaking wastewater. The existence of TBA

or phosphate implied the surface hydroxyl groups played a significant role in the reaction. Ag and Ni worked as the active sites and the efficient cycling of electron between Ag and Ni enhanced the decomposition of ozone and generated more hydroxyl radicals.

Declaration of competing interest

None.

Acknowledgments

This work was supported by National Key R&D Program of China (No. 2018YFC0406300), the operation for central university of Hohai University (No. 2013/B18020148), and A Project Funded by the Priority Academic Program Development of Jiangsu Higher Education Institutions.

REFERENCES

Ding, D., Liu, C., Ji, Y., Yang, Q., Chen, L., Jiang, C., et al., 2017. Mechanism insight of degradation of norfloxacin by magnetite nanoparticles activated persulfate: Identification of radicals and degradation pathway. Chem. Eng. J. 308, 330–339.

Ginni, G., Adishkumar, S., Rajesh Banu, J., Yogalakshmi, N., 2014. Treatment of pulp and paper mill wastewater by solar photo-Fenton process. Desalin. Water Treat. 52, 2457–2464.

Allafchian, A., Bahramian, H., Hossein Jalali, S.A., Ahmadvand, H., 2015. Synthesis, characterization and antibacterial effect of new magnetically core–shell nanocomposites. J. Magn. Mater. 394, 318–324.

Balasamy, R.J., Tope, B.B., Khurshid, A., Al-Ali, A.A.S., Atanda, L.A., Sagata, K., et al., 2011. Ethylbenzene dehydrogenation over FeOx/(Mg,Zn)(Al)O catalysts derived from hydrotalcites: role of MgO as basic sites. Appl. Catal. A-Gen. 398, 113–122.

Chen, W., Westerhoff, P., Leenheer, J.A., Booksh, K., 2003. Fluorescence excitation - Emission matrix regional integration to quantify spectra for dissolved organic matter. Environ. Sci. Technol. 37, 5701–5710.

Chen, Y., Ma, Y., Zhang, C., 2008. Degradation of organic pollutions in wastewater from regenerated papermaking. Environ. Sci. Technol. 31, 127–131.

Jaafarzadeh, N., Ghanbari, F., Ahmadi, M., 2017. Efficient degradation of 2,4-dichlorophenoxyacetic acid by peroxymonosulfate/magnetic copper ferrite nanoparticles/ozone: A novel combination of advanced oxidation processes. Chem. Eng. J. 320, 436–447.

Krejčíková, S., Matějová, L., Kočí, K., Obalová, L., Matěj, Z., Čapek, L., et al., 2012. Preparation and characterization of Ag-doped crystalline titania for photocatalysis applications. Appl. Catal. B-Environ. 111, 119–125.

Kruse, N., Chenakin, S., 2011. XPS characterization of Au/TiO_2 catalysts: Binding energy assessment and irradiation effects. Appl. Catal. A-Gen. 391, 367–376.

Legube, B., Leitner, N.K.V., 1999. Catalytic ozonation: a promising advanced oxidation technology for water treatment. Catal. Today 53, 61–72.

Li, B., Xu, X., Zhu, L., Ding, W., Mahmood, Q., 2010. Catalytic ozonation of industrial wastewater containing chloro and nitro aromatics using modified diatomaceous porous filling. Desalination 254, 90–98.

Li, L., Wang, Y., Zhang, W., Yu, S., Wang, X., Gao, N., 2019. New advances in fluorescence excitation-emission matrix spectroscopy for the characterization of dissolved organic matter in drinking water treatment: A review. Chem. Eng. J. 381, 122676.

Lin, J., Nakajima, T., Jomoto, T., Hiraiwa, K., 2000. Effective catalysts for wet oxidation of formic acid by oxygen and ozone. Ozone: Sci. Eng. 22, 241–247.

Ling, Y., Liao, G., Xie, Y., Yin, J., Huang, J., Feng, W., et al., 2016. Coupling photocatalysis with ozonation for enhanced degradation of Atenolol by Ag-TiO_2 micro-tube. J. Photochem. Photobiol., A 329, 280–286.

Liu, Y., Mao, Y., Tang, X., Xu, Y., Li, C., Li, F., 2017. Synthesis of Ag/AgCl/Fe-S plasmonic catalyst for bisphenol A degradation in heterogeneous photo-Fenton system under visible light irradiation. Chin. J. Catal. 38, 1726–1735.

Lv, A., Hu, C., Nie, Y., Qu, J., 2010. Catalytic ozonation of toxic pollutants over magnetic cobalt and manganese co-doped γ-Fe_2O_3. Appl. Catal. B-Environ. 100, 62–67.

Ma, J., Sui, M.H., Zhang, T., Guan, C.Y., 2005. Effect of pH on MnOx/GAC catalyzed ozonation for degradation of nitrobenzene. Water Res. 39, 779–786.

Marikutsa, A.V., Rumyantseva, M.N., Yashina, L.V., Gaskov, A.M., 2010. Role of surface hydroxyl groups in promoting room temperature CO sensing by Pd-modified nanocrystalline SnO_2. J. Solid State Chem. 183, 2389–2399.

Mittal, V.K., Chandramohan, P., Bera, S., Srinivasan, M.P., Velmurugan, S., Narasimhan, S.V., 2006. Cation distribution in $Ni_xMg_{1-x}Fe_2O_4$ studied by XPS and Mossbauer spectroscopy. Solid State Commun. 137, 6–10.

Mohammed, K.A., Al-Rawas, A.D., Gismelseed, A.M., Sellai, A., Widatallah, H.M., Yousif, A., et al., 2012. . Infrared and structural studies of $Mg_{1-x}Zn_xFe_2O_4$ ferrites. Physica B 407, 795–804.

Nawale, A.B., Kanhe, N.S., Patil, K.R., Bhoraskar, S.V., Mathe, V.L., Das, A.K., 2011. Magnetic properties of thermal plasma synthesized nanocrystalline nickel ferrite ($NiFe_2O_4$). J. Alloys Compd. 509, 4404–4413.

Nawrocki, J., Kasprzyk-Hordern, B., 2010. The efficiency and mechanisms of catalytic ozonation. Appl. Catal. B-Environ. 99, 27–42.

Pokhrel, D., Viraraghavan, T., 2004. Treatment of pulp and paper mill wastewater—a review. Sci. Total Environ. 333, 37–58.

Qi, F., Xu, B.B., Chen, Z.L., Ma, J., 2009. Catalytic ozonation for degradation of 2,4,6-trichloroanisole in drinking water in the presence of gamma-AlOOH. Water Environ. Res. 81, 592–597.

Ren, Y., Chen, Y., Zeng, T., Feng, J., Ma, J., Mitch, W.A., 2016. Influence of Bi-doping on $Mn_{1-x}Bi_xFe_2O_4$ catalytic ozonation of di-n-butyl phthalate. Chem. Eng. J. 283, 622–630.

Ren, Y., Dong, Q., Feng, J., Ma, J., Wen, Q., Zhang, M., 2012. Magnetic porous ferrospinel $NiFe_2O_4$: A novel ozonation catalyst with strong catalytic property for degradation of di-n-butyl phthalate and convenient separation from water. J. Colloid Interface Sci. 382, 90–96.

Saaedi, A., Yousefi, R., Jamali-Sheini, F., Zak, A.K., Cheraghizade, M., Mahmoudian, M.R., et al., 2016. XPS studies and photocurrent applications of alkali-metals-doped ZnO nanoparticles under visible illumination conditions. Physica E 79, 113–118.

Sui, M., Liu, J., Sheng, L., 2011. Mesoporous material supported manganese oxides (MnOx/MCM-41) catalytic ozonation of nitrobenzene in water. Appl. Catal. B-Environ. 106, 195–203.

Sui, M., Sheng, L., Lu, K., Tian, F., 2010. FeOOH catalytic ozonation of oxalic acid and the effect of phosphate binding on its catalytic activity. Appl. Catal. B-Environ. 96, 94–100.

Sun, W.L., Qu, Y.Z., Yu, Q., Ni, J.R., 2008. Adsorption of organic pollutants from coking and papermaking wastewaters by bottom ash. J. Hazard. Mater. 154 (5), 95–601.

Sundararajan, M., Kennedy, L.J., Nithya, P., Vijaya, J.J., Bououdina, M., 2017. Visible light driven photocatalytic degradation of rhodamine B using Mg doped cobalt ferrite spinel nanoparticles synthesized by microwave combustion method. J. Phys. Chem. Solids 108, 61–75.

Suresh, R., Giribabu, K., Manigandan, R., Stephen, A., Narayanan, V., 2014. Fabrication of $NiFe_2O_3$ magnetic nanorods and application to the detection of uric acid. RSC Adv. 4, 17146–17155.

Verwey, E.J.W., Heilmann, E.L., 1947. Physical properties and cation arrangement of oxides with spinel structures I. Cation arrangement in spinels. J. Chem. Phys. 15, 174–180.

Waldron, R.D., 1955. Infrared spectra of ferrites. Phys. Rev. 99, 1727–1735.

Wang, Z., Ma, H., Zhang, C., Feng, J., Pu, S., Ren, Y., et al., 2018. Enhanced catalytic ozonation treatment of dibutyl phthalate enabled by porous magnetic Ag-doped ferrospinel $MnFe_2O_4$ materials: Performance and mechanism. Chem. Eng. J. 354, 42–52.

Wei, C., Wu, H., Kong, Q., Wei, J., Feng, C., Qiu, G., et al., 2019. Residual chemical oxygen demand (COD) fractionation in bio-treated coking wastewater integrating solution property characterization. J. Environ. Manage. 246, 324–333.

Wei, C., Zhang, F., Hu, Y., Feng, C., Wu, H., 2017. Ozonation in water treatment: the generation, basic properties of ozone and its practical application. Rev. Chem. Eng. 33, 49–89.

Yang, X., Zhang, X.L., Wang, Z.W., Li, S., Zhao, J., Liang, G.W., et al., 2019. Mechanistic insights into removal of norfloxacin from water using different natural iron ore - biochar composites: more rich free radicals derived from natural pyrite-biochar composites than hematite-biochar composites. Appl. Catal. B-Environ. 255, 117752.

Yuan, L., Shen, J., Chen, Z., 2013. Catalytic ozonation of p-chloronitrobenzene over pumice-supported zinc oxyhydroxide. Water Sci. Technol. 68, 1895–1900.

Zhang, F., Wei, C., Hu, Y., Wu, H., 2015. Zinc ferrite catalysts for ozonation of aqueous organic contaminants: phenol and bio-treated coking wastewater. Sep. Purif. Technol. 156, 625–635.

Zhang, F., Wei, C., Wu, K., Zhou, H., Hu, Y., Preis, S., 2017. Mechanistic evaluation of ferrite AFe_2O_4 (A = Co, Ni, Cu, and Zn) catalytic performance in oxalic acid ozonation. Appl. Catal. A-Gen. 547, 60–68.

Zhang, L., Liu, H., Wang, Y., Peng, Y., 2020. Compositional characteristics of dissolved organic matter during coal liquefaction wastewater treatment and its environmental implications. Sci. Total Environ. 704, 135409.

Zhang, X., Zhou, G., Xu, J., Bai, G., Wang, L., 2010. Synthesis and photocatalytic activity of co-doped mesoporous TiO_2 on Brij98/CTAB composite surfactant template. J. Solid State Chem. 183, 1394–1399.

Zhao, H., Dong, Y., Wang, G., Jiang, P., Zhang, J., Wu, L., et al., 2013. Novel magnetically separable nanomaterials for heterogeneous catalytic ozonation of phenol pollutant: $NiFe_2O_4$ and their performances. Chem. Eng. J. 219, 295–302.

Zhao, L., Sun, Z., Ma, J., 2009. Novel Relationship between hydroxyl radical initiation and surface group of ceramic honeycomb supported metals for the catalytic ozonation of nitrobenzene in aqueous solution. Environ. Sci. Technol. 43, 4157–4163.

Zhou, J.H., Zhang, Z.P., Wang, S.F., 2011. Study of advanced treatment on biotreated effluent from papermaking wastewater with UV/TiO_2. J. Guangxi Univ. Nat. Sci. Ed. 36, 353–357.